Freeze cast porous membrane catalyst for hydrogen production via oxy-reforming

Freeze cast catalytic membrane for hydrogen production via oxy-reforming

A. Gondolini[1], A. Fasolini[2], E. Mercadelli[1], F.L. Basile[2], A. Sanson[1]

[1] Institute of Science and Technology for Ceramics (ISTEC) of the National Research Council (CNR), Via Granarolo 64, 48018 Faenza (RA), Italy

[2] Department of Industrial Chemistry "Toso Montanari" University of Bologna, Viale del Risorgimento 4, 40136, Bologna, Italy

Keywords: Methane conversion, Oxy-reforming, H_2 production, Smooth thermal profile, Monolith,

Abstract

In this work, porous catalytic membrane with tailored microstructure has been developed for the production of hydrogen from the oxy-reforming process. Porous catalytic membranes have been produced by freeze-casting of ceria-based powders using camphene as solvent. The process parameters have been optimized in terms of type and amount of dispersant to obtain homogeneous and stable ceramic suspension suitable for the process, while the freezing temperature was chosen on the basis of the microstructure and porosity of the final samples. The obtained freeze cast sample produced showed very high levels of porosity (≈ 80%) and good gas permeability (1.0 x 10^{-11} m^2). The ceria-based porous structure produced was finally evaluated as catalyst in high temperature oxy-reforming reaction for hydrogen production from methane showing high methane conversions (up to 90%) and hydrogen production. The use of a unique catalytic membrane other than pelleted catalysts allowed the obtaining of smooth thermal profiles without the evidence of endothermic or exothermic peaks.

1. Introduction

The worldwide urgent environmental concern is a strong incentive for using hydrogen (H_2) as a sustainable and clean energy vector. To date, hydrogen is mainly produced together with CO (syngas) by several reforming processes that use carbon-based feedstock [1]. Among the others, Steam Methane Reforming (SMR) is the primary commercial route for hydrogen production. SMR (Eq. (1)) is carried out at a high temperature (750–850°C) for its endothermicity [2].

$$CH_4 + H_2O \leftrightarrows 3H_2 + CO \qquad (\Delta H^0_{298} = +206 \text{ kJ mol}^{-1}) \qquad (1)$$

The endothermic nature of SMR leads to an important difference between the temperatures of the reactor wall and the catalytic bed, which requires external heating as high as 1100–1200 °C. As a consequence, important stress on the reactor and catalyst occurs affecting their reliability and durability.

To overcome this issue, the exothermic catalytic partial oxidation (CPO, Eq. (2)) can be exploited in the so-called oxy-reforming.

$$CH_4 + 0.5O_2 \leftrightarrows 2H_2 + CO \qquad (\Delta H^0_{298} = -36 \text{ kJ mol}^{-1}) \qquad (2)$$

This process exploits the heat developed by the exothermic CPO to feed the endothermic SMR increasing temperature control and reducing operative temperature in respect to the two separate reactions.

There are many catalysts based on noble metals, such as Ru, Rh, Pt, and Pd, as well as Ni-based catalysts, which are effective in steam-reforming reactions. The metallic catalysts are generally anchored onto ceramic based- catalytic supports (Al_2O_3, SO_2, MgO, CeO_2, and TiO_2) that are produced as porous pellets and loaded into the reactor. Even if a lot of work has been published from the material's point of view in terms of nature of catalysts and supports, synthesis methods,

microstructural/morphology/functional characterizations [3], less studies have been focused on the shaping/structure of the porous oxide substrate. The design of suitable ceramic-based membranes [4–9] and/or porous catalyst [10–14] with a strict control of the pore size and structure can be crucial for practical application and process industrialization. To implement the performance of the reactions, the use of porous catalytic membranes with tailored microstructure has been recently proposed for SMR [15] and SMR combined with the water gas shift [16]. For the shaping of engineered porous ceramic structures, several methods have been reported so far [17]. Organic sacrificial template and direct foaming methods exploit thermally fugitive compounds or gases to produce porosity. The first one, in particular, allows a wide range of porosity level (up to 50%) and pores dimension/morphology by simply tuning the nature and size of the pore former used. However, the main drawbacks related to this technique are i) the long thermal burnout step necessary to completely eliminate the pore formers and ii) the porosity produced is generally not aligned in a specific direction but randomly organized.

To produce samples with aligned and interconnected porosity, replica techniques based on the impregnation of foam structures with ceramic suspension and their subsequent thermal bourn-out, have been developed [17]. With these methods it is possible to obtain a high level of porosity (even higher than 90%). However, long thermal removing step and poor mechanical properties of the final body have been frequently reported [18].

Freeze casting has been recently received particular attention for the production of materials with highly interconnected and organized porosity with improved mechanical strength and better permeability to gas and liquid [19–21]. The general process requires the preparation of a stable suspension of ceramic particles that is cast and subsequently frozen in a mould. The solvent is afterward sublimated and the produced sample is consolidated through a thermal treatment. The obtained structure shows oriented channels due to the replica of the solvent crystals along the freezing direction [20]. Freezing of the ceramic slurry from the bottom induces, as example, the growth of vertically aligned solvent crystals that lead to vertically oriented porosity. The final microstructure of

samples can be engineered for a specific application changing the slurry formulation and the process parameters. However, process parameters such as freezing and sublimation conditions strongly depend on the solvent used for the process. The most common solvent is water that produces a lamellar pore channel microstructure. Other common solvents are tert-butyl alcohol (TBA) and camphene able to produce prismatic and dendritic shape porosities, respectively [21]. The different solvents also lead to different process temperatures. While water and TBA-based slurry can be prepared at room temperature using a conventional ball milling, camphene-based slurries need temperatures between 55-60°C. On the other hand, water and TBA-based slurries require low freezing temperature and pressure while, camphene can be frozen at higher temperature (up to 35-40°C) and, more importantly, sublimated at room temperature and atmospheric pressure [21,22].

The literature about freeze casting for ceramic-based energy devices is up to now limited to some researches about Solid Oxide Cells [23,24], Gas Separation Membranes [25,26] and an example on Membrane Reactors [19]. In these applications, the hierarchically organized and aligned porosity mainly implements gas transport and, as a consequence, the resulting performances, thus boosting the industrialization and commercialization of these devices.

In the case of catalytic applications, while ceramic-based porous catalytic membranes could provide pressure drop one or two orders of magnitude smaller than that of randomly packed pellets enhancing heat distribution and mass transfer [27], freeze cast samples are still largely unexplored [28]. In this work, porous ceramic substrates have been produced by camphene freeze-casting of ceria-based powders to be applied as catalytic membrane in hydrogen production reaction from methane. Gadolinium-doped CeO_2 (GDC) was considered as starting material for its interesting redox properties, high catalytic activity and low deactivation rate for hydrogen production [29–32]. GDC-based slurries were firstly optimized in terms of nature and amount of deflocculant to obtain homogeneous and reproducible samples. Process parameters (temperatures and freezing conditions) have been afterwards evaluated for the development of porous membranes with high level of interconnected porosity. The freeze cast GDC support (impregnated with Rh) was finally tested to

produce hydrogen from oxy-reforming producing high methane and hydrogen conversions with smooth thermal profiles.

2. Material and methods

Freeze-casting slurries were produced using $Ce_{0.8}Gd_{0.2}O_{2-d}$ (GDC 20, FuelCellMaterials, USA) as starting powder, camphene (>95%, Sigma-Aldrich) as solvent and polystyrene (Sigma Aldrich) as binder. A slurry was formulated considering 20vol% of ceramic powder in camphene and 10vol% of polystyrene in respect to the powder. The addition of different types and amounts of deflocculants was considered and evaluated: Brij 58 (Sigma Aldrich, Germany), Phospholan PE65 (Nouryon, Sweden), Glycerin trioleate (GTO Sigma Aldrich, Germany), Hypermer KD1 (Croda, Italy), Polyvinylpyrrolidone (PVP, Mw~29000, Sigma Aldrich, Germany). The slurries were prepared at 55°C, melting firstly the solvent and adding afterwards dispersant and powder. After 30 minutes of stirring, the slurry was sonicated (Sonicator, ultrasonic processor XL, USA) for 5 minutes. After this process, polystyrene was added to the GDC 20 suspension and the whole system was stirred for 90 minutes. The as-prepared slurry was then poured into a circular crown silicon mold supported on metal plate kept at 0°C to obtain vertically aligned porosity. The cast samples were demolded after 30 minutes from casting and left for 3 days at room temperature to obtain the complete sublimation of the camphene. The samples were then thermally treated at 1400°C for 4 hours to produce the final GDC membranes, 2 cm height and with 1.4 cm of diameter.

2.1.Characterization methods

The size distributions of the GDC powder in the camphene using different deflocculants were registered at 55°C using a dynamic light scattering analyzer (DLS Nano S, Malvern UK) after a sonication treatment of 5 minutes in a sonication bath. For the first tests, samples with 4vol% of powder and deflocculant concentration of 10vol% in respect to the powder were considered and diluted 400 times for DLS measurements. Each measurement was the average of 15 performed

analyses and was repeated 3 times. Viscosity measurements of as-produced suspensions were performed using a controlled-stress rheometer (BohlinCVOR 120, Malvern Instruments) equipped with serrated plates (diameter = 20 mm). All the measurements were performed at 55°C setting the distance between the plates at 500 µm. The samples for viscosity test contain the same concentration of powder of the cast slurry and a fixed amount of 10vol% of deflocculants.

The final microstructure was investigated by scanning electron microscopy (Field Emission Gun - Scanning Electron Microscopy, FEG-SEM, ΣIGMA, Zeiss, Germany). The cross-section surface of the sample was firstly embedded under vacuum in epoxy resin and then mechanically polished till 0.25 µm finishing. Porosimetric analyses of the substrates were carried out by mercury intrusion technique using Thermo Finningan Pascal 140 working at pressure from ambient to 400 kPa for pores with diameter in the range between 3 and 1000 µm. The permeability test was performed in an in-house testing rig using N_2 and applying the Darcy's Law. The air permeability value was calculated using the equation reported by Simwonis et al. [33,34].

2.2.Catalytic tests

The GDC membrane was impregnated with Rh nitrate (~10 wt% Rh in > 5 wt.% in HNO3 – BASF) by incipient wetness impregnation, using an aqueous-acetone mixture (volume ratio 1:1). The use of acetone was found to be necessary to reduce the viscosity of the solution and allows a homogeneous dispersion of the Rh-containing solution inside the membrane porosity. The impregnation was followed by a drying step at 120°C and calcination at 500°C, to produce rhodium oxide by decomposition of the Rh precursor. The final metallic Rh loading was 0.5%, expressed as grams of metallic Rh over grams of support. In a typical experiment 1,80 grams of catalyst were employed. The catalytic tests were carried out in a continuous tubular quartz reactor with an internal diameter of 14 mm, where reduction was performed before the catalytic tests by heating the catalyst to 750°C under hydrogen (50 ml/min) and keeping it at this temperature for 1 h. The impregnated membrane catalyst, which consisted in a cylindrical monolith with a diameter of 14mm, was fitted inside the

quartz tube, so that its aligned porosity allowed the fed gas to flow through it. A sliding thermocouple placed in a 2 mm hole in the middle of the membrane was used to measure the temperature of the monolith. The oxy-reforming process was performed feeding a mixture of methane, oxygen and steam at different temperatures and steam to methane (S/C) ratios. Deionized water was feed by a JASCO HPLC pump and fully vaporized before mixing with preheated O_2 and CH_4. The effluent wet gaseous mixture (H_2, CO, CO_2, non-converted CH_4 and vapor) was fed to a condenser maintained at about 0 °C in order to eliminate water vapor. The dry gas mixture (DG) was analyzed on-line by an Agilent 490 micro gas chromatograph. Two catalytic tests were performed feeding a mixture of methane, oxygen and steam or methane and steam, to perform the oxy-reforming [35,36] and catalytic partial oxidation [37,38] processes respectively. In the oxy-reforming process, the feed composition was adjusted to obtain a mixture with sub-stoichiometric ratio of H_2O and O_2, namely an O_2/C ratio of 0.21 and a S/C ratio of 0.70. The influence of temperature (550°C; 600°C; 650°C; 700°C and 750°C)was investigated at S/C of 0.7, while the effect of S/C (0.7; 1.0; 1.5; 2.0; 3.0) was studied at 750°C. Methane inlet flow was kept constant while S/C was increased which resulted in an increase of the total inlet flux, hence of the gas hourly space velocity (GHSV). On the opposite, the O_2/C ratio was increased to 0.50 while the S/C was decreased to 0.50 in the catalytic partial oxidation experiments carried out at 750°C.

Table 1 shows the reaction conditions used.

The monolithic membrane catalyst produced in this work (with a 0.5% Rh loading) was compared with a reference catalyst, i.e. a more classical catalytic configuration, in the form of pellets. In fact, CeGd powder, not submitted to freeze casting, was impregnated with the same amount of Rh and shaped in pellets (0.84-1.41 mm). The same weight of catalyst was loaded into the reactor for both monolith and pellets to compare catalysts with the same amount of Rh. The catalysts were compared in the oxy-reforming process at 750°C, 1 atm, O/C 0.2 and S/C 0.7, which resulted in a weight hourly space velocity (WHSV) of 1.50 $l \cdot h^{-1} \cdot g\ cat^{-1}$ for both catalytic systems.

Table 1. Operative conditions employed in the catalytic tests.

Operative Parameter	**Oxy-reforming**	**Catalytic Partial Oxidation**
Temperature (°C)	550; 600; 650; 700; 750	750
Pressure (atm)	1	1
GHSV (h^{-1})	2900; 3400; 4150; 4900; 6450	3100
W**HSV (l·h^{-1}·g cat^{-1})**	1.5; 1.74; 2.15; 2.53; 3.31	1.6
Methane feed (ml/min)	24	0.5
Oxygen to carbon ratio (O_2/C)	0.21	0.5
Steam to carbon ratio (S/C)	0.7; 1.0; 1.5; 2.0; 3.0	0.5

The results were expressed in terms of methane conversion that was taken as reference to evaluate the activity of the catalyst. It was compared with the conversion calculated at the thermodynamic equilibrium. The CEA-NASA software was employed to obtain the outlet composition at the thermodynamic equilibrium. The software gives the molar gaseous outlet composition (non-converted CH_4 and H_2O, CO, CO_2, H_2 and deposited carbon if present), starting from the feed composition in terms of molar percentage, the reaction temperature and pressure.

3. Results and discussion

3.1.Membrane synthesis

The suspension and process parameters for the production of GDC membrane were firstly studied and optimized, starting from the nature and amount of deflocculant needed for the production of a stable camphene-based slurry. The type of deflocculant has to be chosen taking into account the

nature of the dispersing medium and the slurry preparation conditions. Camphene is a non-polar solvent than should be used at temperature higher than 45°C to assure a liquid state. Furthermore, its high volatility can hinder a homogeneous porous structure along the entire thickness during the freezing step. For these reasons, all the analyses and processes done in the frame of this work were carried out at 55°C and in closed chamber. The non-polar nature of the solvent lead to consider deflocculants with a mainly steric action. This stabilization mechanism is generally assured by long chain molecules or polymers, which can remain free in the dispersing medium. These systems are characterized by an anchoring group that enable the interaction with the particle surface, and the length of the adsorbed chains that must be long enough to provide the desired hindrance effect [39]. The Brij 58, Phospholan PE65, Glycerin trioleate, Hypermer KD1 and Polyvinylpyrrolidone deflocculants were tested in this study as it is reported in the Experimental part. As reported by Moreno [39] the stability of a suspension can be evaluated using different techniques such as particle size, zeta potential, sedimentation and rheological behaviour. Due to the non-polar nature of the solvent, particle size and rheological tests were selected to determine the stabilizing capability of each deflocculant.

Figure 1, shows DLS values of powder mean diameters recorded for camphene suspensions with different deflocculants. Particularly, Phospholan PE65, glycerine trioleate (GTO) and Hypermer KD1 showed the lower particle mean sizes (ranging from 730 to 810 nm), indicating the better ability of these deflocculants to disperse particles. It is important to note that these values are higher than the aggregates sizes shown in the SEM micrographs of the powder (Figure 2). DLS analysis registers, in fact, a hydrodynamic diameter of the moving unit inside the solvent [40,41], that includes the deflocculant adsorbed on the particle surface and the coordination sphere. The lower mean particle sizes for Phospholan PE65, glycerine trioleate (GTO) and Hypermer KD1 can be ascribed to the better absorption capacity of these deflocculants on the powder surface [39]. On the contrary, Brij58 and polyvinylpyrrolidone (PVP) show size values comparable or slightly lower to the sample without

a deflocculant component indicating the insufficient dispersing and/or anchoring ability of these agents.

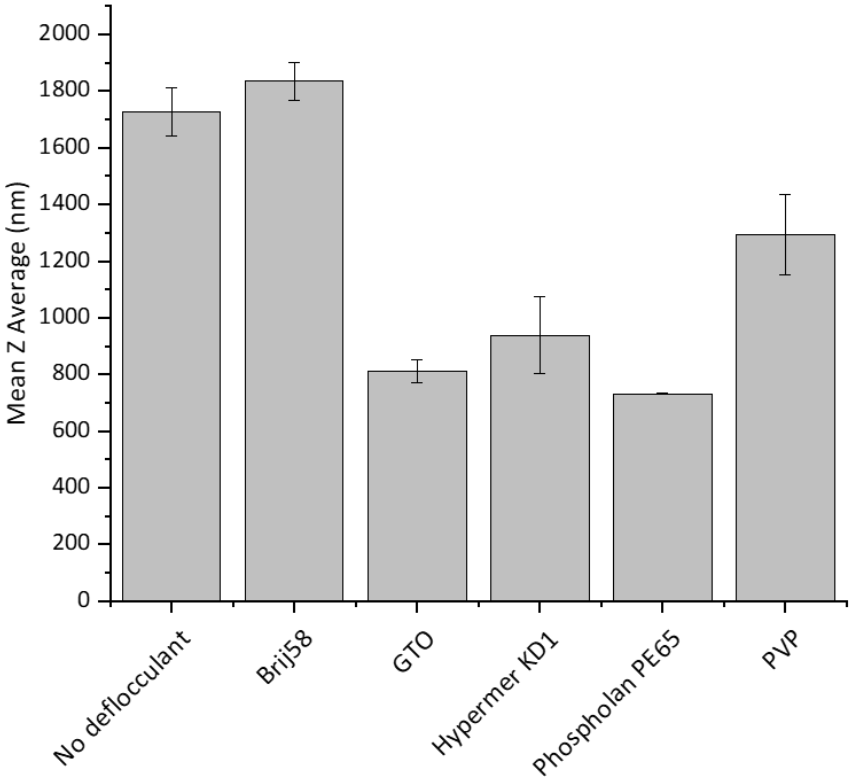

Figure 1. Mean particle size of the powder-deflocculant suspension evaluated using DLS analysis.

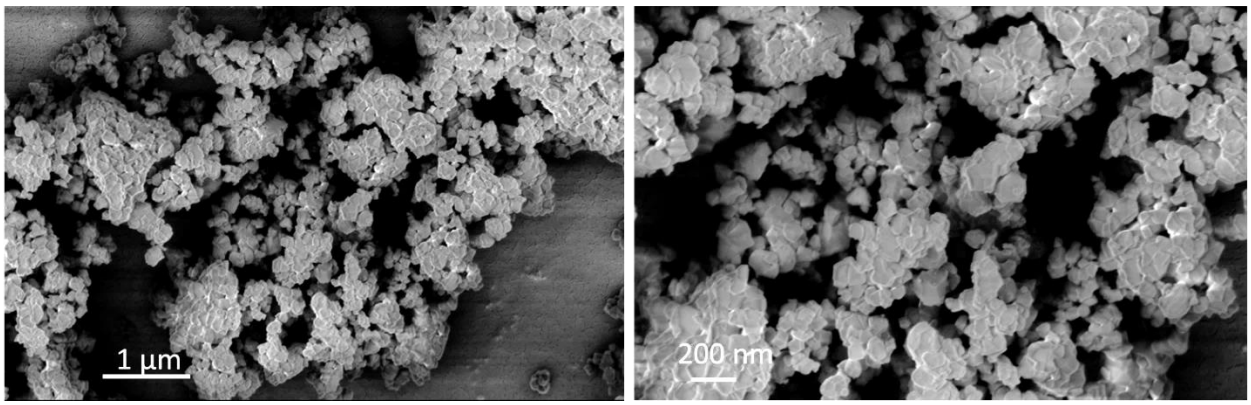

Figure 2. SEM micrographs of the GDC 20 powder used in this study.

It must be noted that particle size is measured with very dilute suspensions [39,41]. Since the solid loading increases the interactions among particles, viscosity measurements using suspensions with the same powder concentration of the freeze casting slurry were considered to test the best dispersing properties of deflocculants in real conditions.

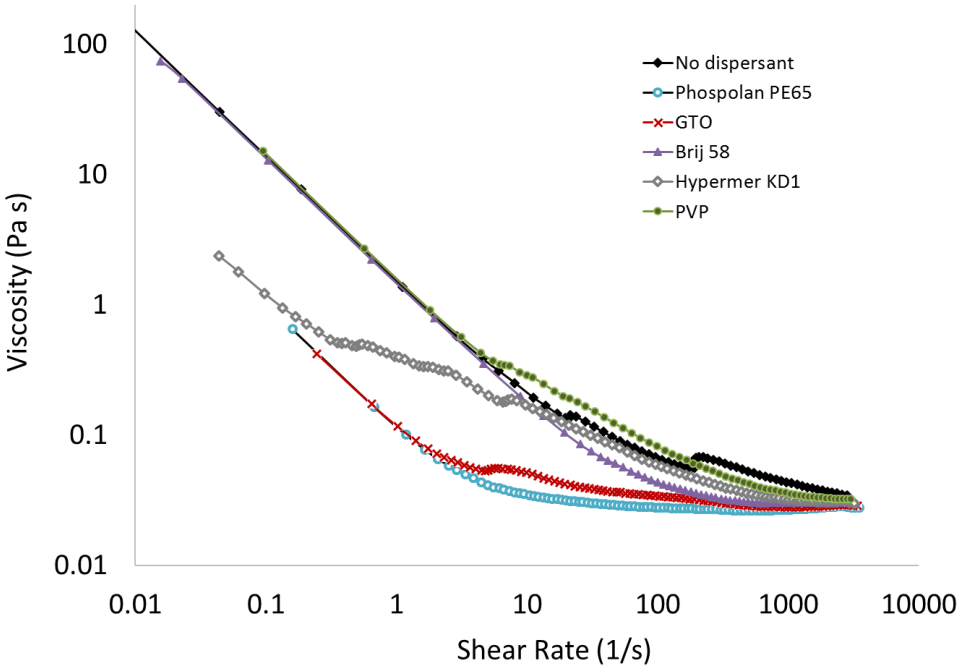

Figure 3. Viscosity values of the GDC 20 slurries containing the different deflocculants.

The registered viscosity curves (Figure 3) show a pseudoplastic behaviour for all the considered slurries. In particular, the lower viscosity recorded for Phospholan PE65 and GTO suspensions, indicates the better stabilization ability of these deflocculants confirming the trend previously showed by DLS analyses (Figure 1). On the contrary to what expected, the suspension containing Brij58 presents good stabilizing properties, at high shear rate, probably due to the alignment of the long hydrophobic alkyl chains that leads to an increased lubrication of the system. Conversely, the suspension with PVP shows the highest viscosities for all the range of shear rates values considered, due to the polymeric nature of the deflocculant that, in concentrated suspension, increases the system viscosity.

Among the others, Phospholan PE65 shows the best stabilizing ability and, for this reason, was selected as deflocculant for the GDC slurry. The viscosities determined in suspensions for different concentration of Phospholan PE65 in respect to the powder (Figure 4a) show an optimal deflocculant concentration between 5 and 10 vol% in respect to the powder. By DLS measurements a scan from 5 to 10vol% of deflocculant was considered and the optimal concentration was assessed to be equal to 6%, corresponding to the lowest value of mean particle size registered (Figure 4b). This deflocculant amount was, therefore, selected for the production of the freeze cast slurries.

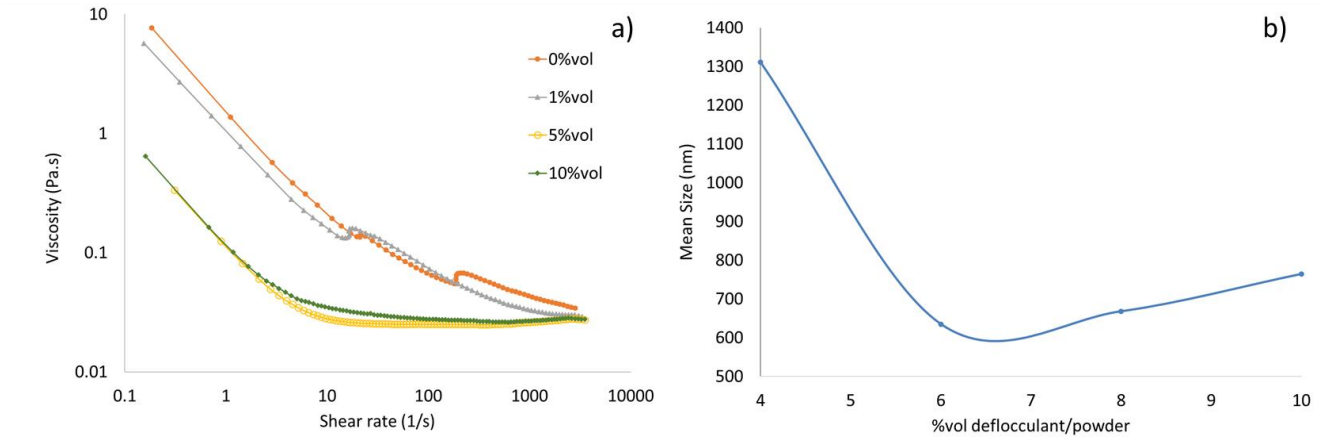

Figure 4. Viscosity of the GDC 20 slurries a) and mean size of the suspensions b) containing different amounts of Phospholan PE65.

Cylindrical membranes were produced by directional freeze casting keeping the bottom part of the mould at 0°C. The sintered samples show a high level of porosity (74.7 ± 0.2) vertically aligned (Figure 5) with a pore diameter of 7.1 ± 0.1 µm.

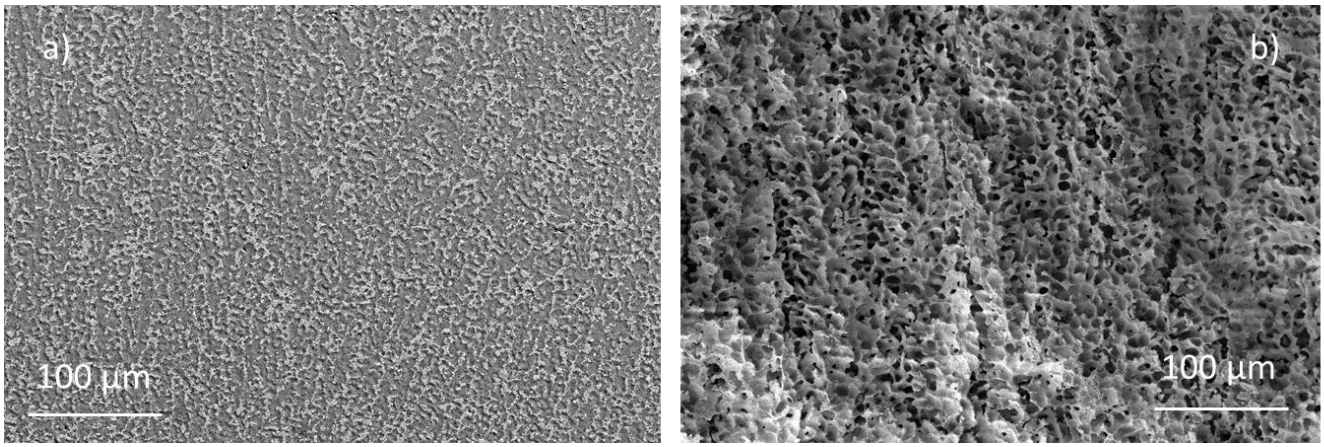

Figure 5. SEM micrographs of the a) polished and b) fresh fracture of the sample produced by directional freeze casting.

As reported elsewhere [21,22,42], one of the main issues linked to the production of freeze cast supports is the production of non-homogeneous microstructure along the sample's height due to inhomogeneous temperature gradient. To check this effect, the cross section of the samples produced were analysed in different positions along the sample height. The membranes show four regions with different microstructures: the bottom, in contact with the cooling metallic surface (I), the central body showing two different structure of porosity (II and III) and the top surface, in contact with air during the freezing (IV). The specific microstructures of each region are shown in Figure 6.

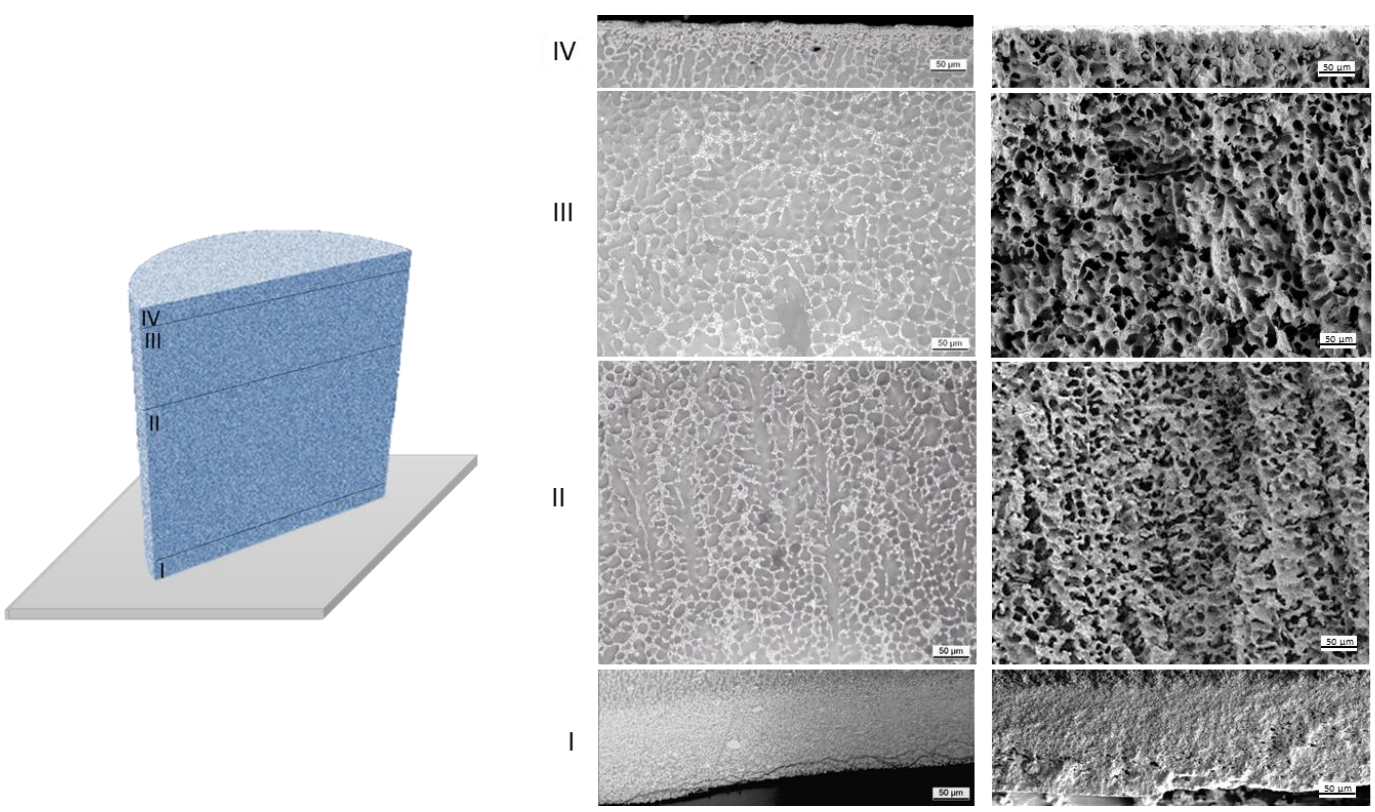

Figure 6. SEM micrographs of the polished (on the left) and fresh fracture (on the right) at different height of the freeze cast sintered sample.

The bottom part of the sample shows a dense layer of 150-200μm due to the rapid solidification of suspension that probably hinder particles rearrangements in the first micrometres of the membrane. In zone II (Figure 6), dendritic aligned porosity structures typical of camphene crystal formation were formed [21,43,44] with a preferential orientation. Beyond the zone II, the temperature gradient further decreases producing a second dendritic growth (part III) coming from the primitive dendritic arms, resulting in the formation of equiaxed pore structures [22]. As the temperature gradient decreases, in fact, more time the camphene molecules have to diffuse and form dendritic crystal. Finally, the upper part of the sample shows a 15-20 μm thick dense layer attributed to the fast evaporation of melted camphene from the sample surface in the early stage of freezing, resulting in a layer with high solid content [21,22]. Some authors [43], exploit this fast evaporation related to the relatively high vapour pressure of camphene [21], to produce asymmetric porous-dense microstructures, engineering the dense layer thickness by the control of process parameters during freezing. However, for the development of catalytic membranes, an open pore structure is crucial to assure the permeability of gases inside the catalytic supports [28]. For this reason, the process parameters were changed to produce samples without a densified layer. Since the formation of the bottom dense layer is attributed to the fast freezing in that part of the sample, the freezing temperature was increased in order to decrease the temperature gradient along the sample. In particular, since the camphene melts between 44-48°C, temperatures of 5 and 35°C were selected for the study of the freezing process. As shown in Figure 7, using a freezing temperature of 5°C (Figure 7 b) the GDC support shows bottom dense layer of reduced thickness (30-50 μm) in respect of sample frozen at 0°C (Figure 7a). Furtherly increasing the temperature to 35°C (Figure 7 c), completely avoided the formation of dense layer i and the bottom part of the sample (Figure 7 d) shows an open porous microstructure appropriate to gas permeation. 35°C was then selected as freezing temperature for the production of the next samples. In the same way, the process conditions to avoid the formation of the upper dense layer was studied. More specifically, the formation of this layer is attributed to the evaporation of melted camphene during the first part of the freezing. To reduce the evaporation speed, the sample was frozen

in a chamber saturated of solvent (Figure 8 b) producing, in this way, upper dense layer thinner (of few micrometres) in respect to the 0°C sample (Figure 8 a). GDC support without upper dense layer was obtained casting the slurry in a mould placed inside a water bath (at 35°C), with the water level higher than the mold height. In this way, the head of water on the top of the sample completely avoid the solvent evaporation during freezing producing homogeneous open cellular structures in the entire volume.

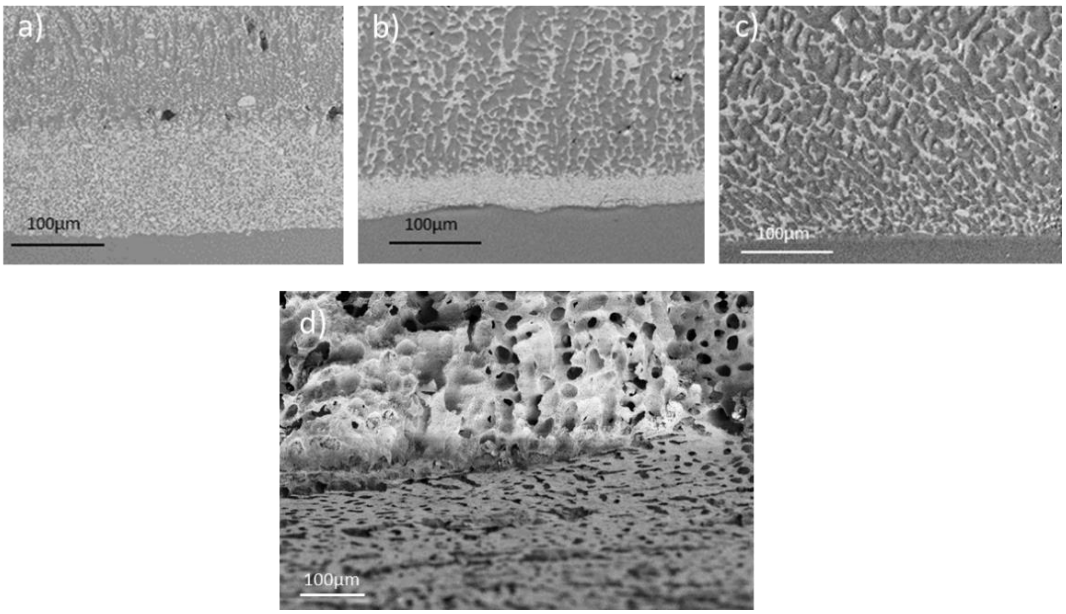

Figure 7. SEM micrographs of the polished fractures of the bottom part of samples frozen at a) 0°C, b) 5°C and c) 35°C. Figure d) is a fresh fracture of the sample frozen at 35°C.

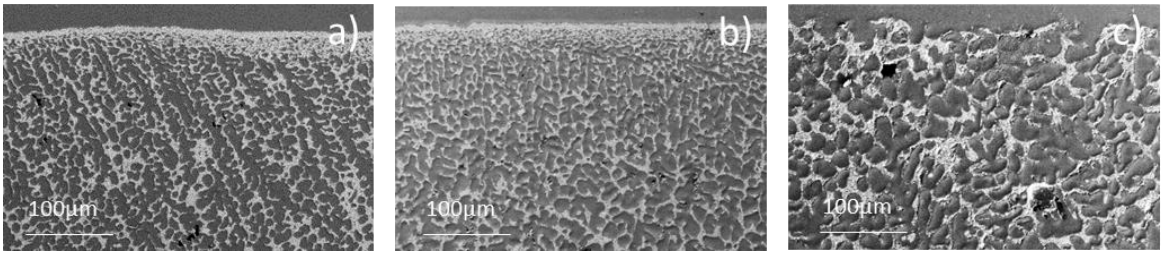

Figure 8. SEM micrographs of the polished fractures of the upper part of samples frozen at 35°C a) in air, b) in camphene saturated chamber and c) in water bath.

Increasing the freezing temperature, the total volume of porosity and the mean pore diameter of samples increases, as shown in Table 2 and Figure 9 a). This phenomenon is well known in literature: as reported by Deville [21] a faster freezing rate leads to the formation of a finer microstructure and, therefore, a finer porosity. In the same way, the cooling rate has also a slight effect on the pore volume. The sample frozen at 35°C in a water bath, shows narrower pore size distribution (Figure 9 a), confirming the superior homogeneity of the microstructure of this sample in respect to the ones cast at 0 and 5°C. On the other hand, the sample frozen at 0°C shows the widest pore size distribution due to the different freezing speed along the sample height, confirming the morphological data (Figure 6) previously discussed. The gas permeability level of the supports (Table 2 and Figure 9 b) increases in accordance to the sample's porosity confirming a higher permeability of the membrane frozen at 35°C, in water bath. This sample was, therefore, selected for the next catalytic tests.

Table 2. Values of porosity, mean pore diameter and permeability of the produced samples.

Freezing Temperature (°C)	**Porosity (%)**	**Mean pore diameter (μm)**	**Permeability (m^2)**
0	74.7 ± 2.0	7.1 ± 0.1	3.9×10^{-12}
5	76.7 ± 3.0	11.8 ± 0.6	8.3×10^{-12}
35	79.7 ± 1.6	14.3 ± 0.4	1.0×10^{-11}

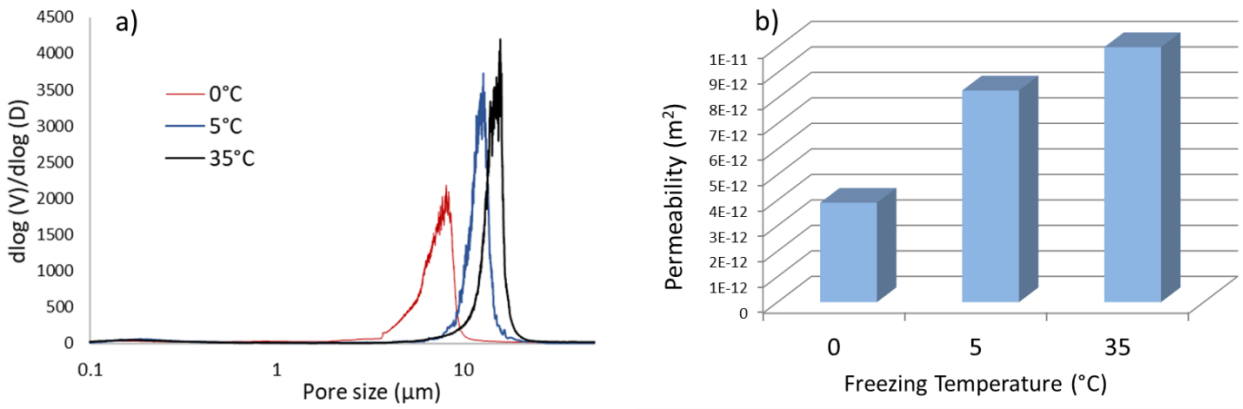

Figure 9. Pore size distribution a) and Darcy permeability values b) of the produced samples

3.2.Catalytic tests

To test the catalytic properties of the selected membrane catalyst in oxy-reforming, the influence of the oven temperature on the performances was firstly studied at S/C of 0.7 and O/C of 0.2. As shown in Figure 10, a methane conversion of 46%, slightly lower than the equilibrium one (52%), was obtained at 550°C. In these conditions, the equilibrium is not reached in the system due to the low temperature employed for the oxy-reforming process, which limits the kinetic of the catalyst. A hydrogen production of 0.7 l/h was obtained.

Increasing the reaction temperature promotes the catalytic activity (Figure 10) leading to higher experimental and equilibrium methane conversions. The equilibrium conversion is reached for temperature equal and above 650°C with the highest value of conversion (90%) obtained at 750°C. High level of conversions could be obtained even at lower S/C and O/C values. The use of low S/C may lead to a cheaper process in terms of reactor volume and steam cost, with respect to the classical industrial steam reforming, which is usually carried out at S/C above 3 [45]. Hydrogen production was also raised for the same reason, reaching 1.6 l/h at 650° and 2.7 l/h at 750°C.

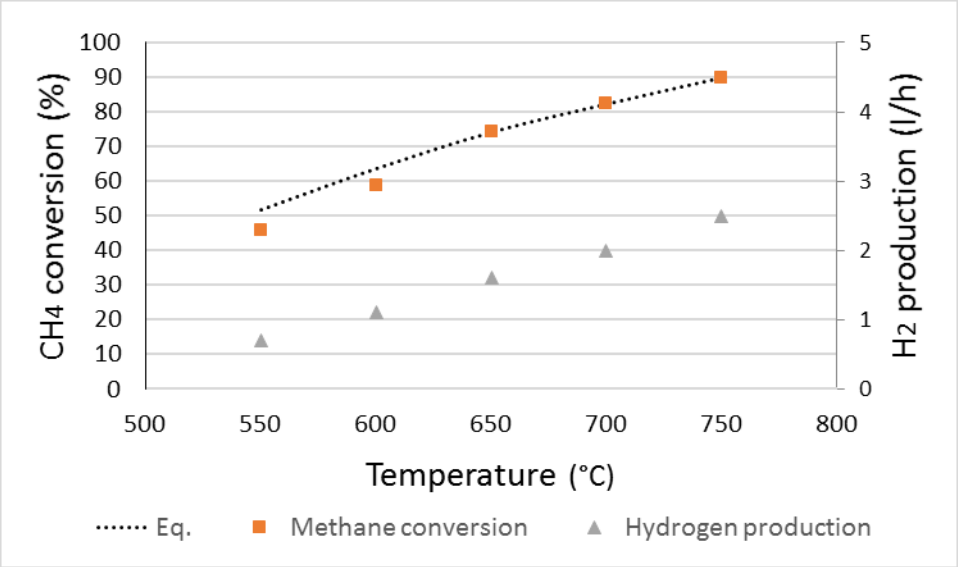

Figure 10. Methane conversion, equilibrium methane conversion and hydrogen production obtained at S/C 0.7, O/C 0.2, 1 atm, GHSV 2900 h^{-1} and different temperatures.

In order to study the effect of steam concentration on the catalytic activity, the S/C was increased maintaining at 750°C the reaction temperature (Figure 11). At low S/C, the equilibrium is reached at 90% conversion. Increasing the S/C, the equilibrium conversion raises due to the higher amount of steam (reagent of the SR reaction). However, a slighter increase is observed for the experimental conversions. This is due to the fact that SR and CPO kinetics are controlled by the rate-determining step of methane decomposition to adsorbed carbon atoms [46]. As the methane to Rh ratio is not varied in these tests, the activity of the catalyst, hence the conversion, only slightly varies with the presence of steam.

Nevertheless, the increase in conversion raises the hydrogen production from 2.7 at S/C 0.7 to 3.1 l/h at S/C 1.5 and S/C 2 and 3.2 l/h at S/C 3. Thus, hydrogen production can be increased by increasing the amount of steam fed. However, a plateau is reached at high steam to methane ratios. Since the increasing of the steam amount raises the process cost, S/C 1.5 seems to be an optimum compromise between the hydrogen productivity and operating cost.

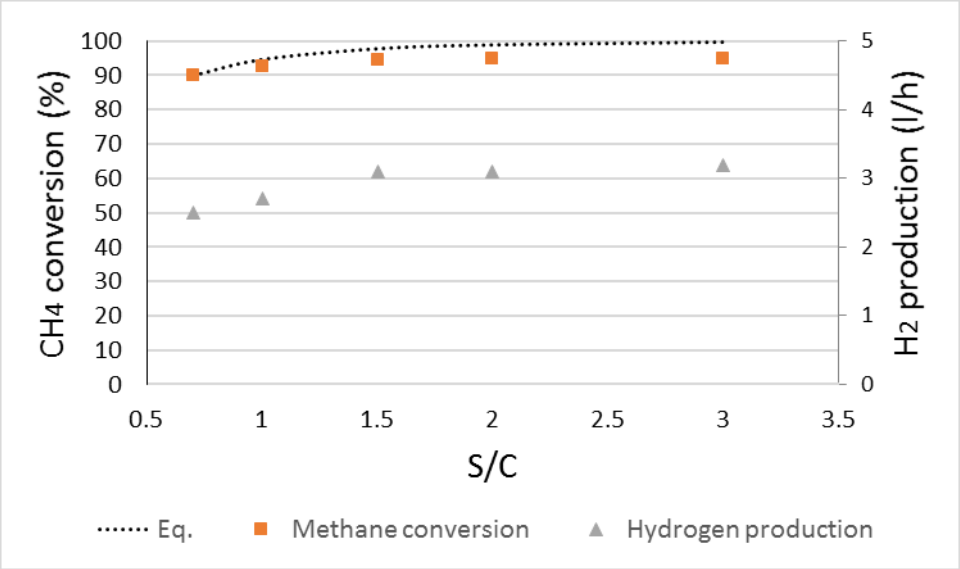

Figure 11. Methane conversion, equilibrium methane conversion and hydrogen production obtained at 750°C, O/C 0.21, 1 atm, and S/C 0.7 (GHSV=2900 h^{-1}), 1.0 (GHSV=3400 h^{-1}), 1.5 (GHSV=4150 h^{-1}), 2.0 (GHSV=4900 h^{-1}) and 3.0 (GHSV=6450 h^{-1}).

Interestingly, small temperature variations were observed over the structured catalyst. In fact, the temperature along the catalytic bed was found to be homogeneous, with variations of less than 8°C over the catalyst. In general, catalytic bed temperatures are slightly lower than the oven temperature, as the thermocouple is placed in the middle of the reactor, over the catalyst. There, the endothermic SR, which is the predominant reaction that takes place in oxy-reforming, contributes to lower the temperature by approximately 10°C. The employment of a unique ceramic membrane in respect to pelleted catalysts, favours heat transfer and allows to obtain smooth thermal profiles without endothermic or exothermic peaks (Figure 12), which can be produced in the oxy-reforming process [47,48]. To further confirm this, the oxy-reforming reaction was carried out at 750°C and S/C 0.7 over analogous pelleted catalyst. The results of the test in terms of conversion are reported in Table 3 while the thermal profiles of the catalytic bed are shown in Figure 12b. The two catalytic membranes show similar conversions as the equilibrium was reached in all cases thanks to the favourable conditions. However, it is interesting to see that different thermal profiles were developed over the

catalytic bed (Figure 12b). In particular, a higher temperature was recorded in the case of the pelleted catalyst, in particular at the beginning of the catalytic bed. This trend is due the occurrence of the exothermic CPO at the beginning of the catalytic bed and of the endothermic steam reforming at the end of it, which can cause a different heat distribution over the catalytic bed with hot spots in its first part. The use of a structured membrane catalyst allowed to homogenously distribute the heat and lower the catalytic bed temperature, thanks to the absence of grain boundary which favoured heat exchange [49].

A homogeneous temperature profile was obtained even when the S/C was decreased from 0.7 to 0.5 and the O/C was increased from 0.2 to 0.5, in an oxygen-enriched oxy-reforming. In this case a higher bed temperature was recorded due to the increased amount of oxygen which favoured the exothermic CPO. The difference in catalytic bed length was caused by the different apparent density of the two catalytic membranes. The absence of hotspots over the freeze cast membranes is helpful in decreasing catalyst deactivation and runaway risk [50].

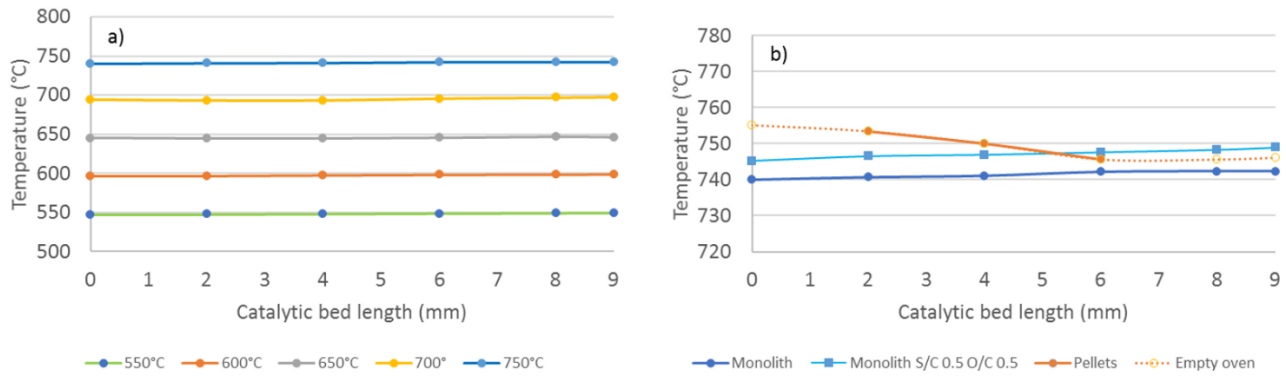

Figure 12. Catalytic bed temperature profile at different conditions varying the oven temperature (a) and the catalyst (b).

Table 3. Experimental and equilibrium conversion obtained by the catalytic membrane and pelleted catalyst in oxy-reforming at 750°C with S/C 0.7 and O/C 0.2 or S/C 0.5 and O/C 0.5.

Catalyst	**750°C; S/C 0.7; O/C 0.2**

	Exp. conversion	Eq. conversion	WHSV ($l \cdot h^{-1} \cdot g\ cat^{-1}$)	GHSV (h^{-1})
Monolith	90	90	1.50	2900
Pelleted	89	89	1.50	4100

4. Conclusions

In this work, GDC-based membranes were successfully produced by camphene freeze casting through an accurate study of suspension stability and process parameters. Phospholan PE65 was selected as best deflocculant in amount equal to 6 vol% in respect to the powder to provide the best slurry stabilization. Inhomogeneous heat transfer inside the sample causes changes in the microstructure and porosity along the sample height: sample with dense layer, aligned dendritic channel and equiaxed pore were produced freezing the bottom part of the sample at 0°C. The formation of the upper dense layer was linked to the fast camphene evaporation during freezing. The presence of a dense layers was completely avoided increasing the freezing temperature at 35°C and casting sample in a water bath to hinder camphene evaporation. Catalytic membranes produced in this way showed high values of porosity, permeability and homogeneous microstructure. The possibility to exploit freeze cast GDC catalyst in high temperature oxyreforming reaction for hydrogen production from methane has been evaluated. High methane conversions, close to the equilibrium value, and high hydrogen production are obtained in different reaction conditions. In addition, the use of a unique ceramic membrane in respect to pelleted catalysts allows a smooth thermal profiles without the evidence of endothermic or exothermic peaks. As preliminary study, it has to be noted that low methane fluxes were employed reducing methane conversion and heat development compared to conventional low contact time operations. Future works, will be focused on the production of

membrane with low pressure drops, able to sustain high fluxes of reagents, similar to industrial conditions.

5. Acknowledgments

This work has been funded by the agreement between the Italian Ministry of Economic Development and the Italian National Research Council 'Ricerca di sistema elettrico nazionale' PT 2019-2021.

6. References

[1] Membrane Separations Technology, Volume 2 - 1st Edition, (n.d.). https://www.elsevier.com/books/membrane-separations-technology/noble/978-0-444-81633-7 (accessed June 9, 2020).
[2] T.L. LeValley, A.R. Richard, M. Fan, The progress in water gas shift and steam reforming hydrogen production technologies – A review, International Journal of Hydrogen Energy. 39 (2014) 16983–17000.
[3] N.S.N. Hasnan, S.N. Timmiati, K.L. Lim, Z. Yaakob, N.H.N. Kamaruddin, L.P. Teh, Recent developments in methane decomposition over heterogeneous catalysts: an overview, Mater Renew Sustain Energy. 9 (2020) 8. https://doi.org/10.1007/s40243-020-00167-5.
[4] K. G. Beltsios, T. A. Steriotis, K. L. Stefanopulos, N. K. Kanellopulos, Handbook of porous solids. Membrane technology Vol. 4, ed. F. Schuth, K. S.W. Sing J. Weitkamp. Wiley-VCH, Weinheim, (2002), 2281-2433
[5] D. Fino, S. Bensaid, M. Piumetti, N. Russo, A review on the catalytic combustion of soot in Diesel particulate filters for automotive applications: From powder catalysts to structured reactors, Applied Catalysis A: General. 509 (2016) 75–96. https://doi.org/10.1016/j.apcata.2015.10.016.
[6] N. Gao, W. Fan, Z.-K. Xu, Ceramic membrane with protein-resistant surface via dopamine/diglycolamine co-deposition, Separation and Purification Technology. 234 (2020) 116135. https://doi.org/10.1016/j.seppur.2019.116135.
[7] A. Almojjly, D. Johnson, N. Hilal, Investigations of the effect of pore size of ceramic membranes on the pilot-scale removal of oil from oil-water emulsion, Journal of Water Process Engineering. 31 (2019) 100868. https://doi.org/10.1016/j.jwpe.2019.100868.
[8] Status review on membrane systems for hydrogen separation (Technical Report) | ETDEWEB, (n.d.). https://www.osti.gov/etdeweb/biblio/20544843 (accessed April 24, 2020).
[9] E. Mercadelli, A. Gondolini, D. Montaleone, P. Pinasco, S. Escolástico, J.M. Serra, A. Sanson, Production strategies of asymmetric BaCe0.65Zr0.20Y0.15O3-δ – Ce0.8Gd0.2O2-δ membrane for hydrogen separation, International Journal of Hydrogen Energy. 45 (2020) 7468–7478. https://doi.org/10.1016/j.ijhydene.2019.03.148.
[10] H. Lee, M. Yanilmaz, O. Toprakci, K. Fu, X. Zhang, A review of recent developments in membrane separators for rechargeable lithium-ion batteries, Energy Environ. Sci. 7 (2014) 3857–3886. https://doi.org/10.1039/C4EE01432D.
[11] P. A. Connor, X. L. Yue, C. D. Savaniu, R. Price, G. Triantafyllou, M. Cassidy, G. Kerherve, D. J. Payne,R. C. Maher, L. F. Cohen, R. I. Tomov, B. A. Glowacki, R. V. Kumar, J. T. S.

Irvine, Tailoring SOFC Electrode Microstructures for Improved Performance Adv. Energy Mater. 8 (23) (2018), 1800120.
[12] P. Ho, W. De Nolf, F. Ospitali, A. Gondolini, G. Fornasari, E. Scavetta, D. Tonelli, A. Vaccari, P. Benito, Coprecipitated-like hydrotalcite-derived coatings on open-cell metallic foams by electrodeposition: Rh nanoparticles on oxide layers stable under harsh reaction conditions, Applied Catalysis A: General. 560 (2018). https://doi.org/10.1016/j.apcata.2018.04.014.
[13] A. Gondolini, E. Mercadelli, A. Sangiorgi, A. Sanson, Integration of Ni-GDC layer on a NiCrAl metal foam for SOFC application, Journal of the European Ceramic Society. 3 (2017) 1023–1030. https://doi.org/10.1016/j.jeurceramsoc.2016.09.021.
[14] A. Gondolini, E. Mercadelli, G. Constantin, L. Dessemond, V. Yurkiv, R. Costa, A. Sanson, On the manufacturing of low temperature activated Sr0.9La0.1TiO3-δ-Ce1-xGdxO2-δ anodes for solid oxide fuel cell, Journal of the European Ceramic Society. 38 (2018) 153–161. https://doi.org/10.1016/j.jeurceramsoc.2017.07.035.
[15] S.M. Lee, J.M. Won, G.J. Kim, S.H. Lee, S.S. Kim, S.C. Hong, Improving carbon tolerance of Ni-YSZ catalytic porous membrane by palladium addition for low temperature steam methane reforming, Applied Surface Science. 419 (2017) 788–794. https://doi.org/10.1016/j.apsusc.2017.05.039.
[16] D.-W. Lee, S.-J. Park, C.-Y. Yu, S.-K. Ihm, K.-H. Lee, Study on methanol reforming–inorganic membrane reactors combined with water–gas shift reaction and relationship between membrane performance and methanol conversion, Journal of Membrane Science. 316 (2008) 63–72. https://doi.org/10.1016/j.memsci.2007.12.050.
[17] T. Ohji, M. Fukushima, Macro-porous ceramics: processing and properties, International Materials Reviews. 57 (2012) 115–131. https://doi.org/10.1179/1743280411Y.0000000006.
[18] A.R. Studart, U.T. Gonzenbach, E. Tervoort, L.J. Gauckler, Processing Routes to Macroporous Ceramics: A Review, Journal of the American Ceramic Society. 89 (2006) 1771–1789. https://doi.org/10.1111/j.1551-2916.2006.01044.x.
[19] C. Gaudillere, J.M. Serra, Freeze-casting: Fabrication of highly porous and hierarchical ceramic supports for energy applications, Boletín de La Sociedad Española de Cerámica y Vidrio. 55 (2016) 45–54. https://doi.org/10.1016/j.bsecv.2016.02.002.
[20] C. Gaudillere, J. Garcia-Fayos, J.M. Serra, Enhancing oxygen permeation through hierarchically-structured perovskite membranes elaborated by freeze-casting, J. Mater. Chem. A. 2 (2014) 3828–3833. https://doi.org/10.1039/C3TA14069E.
[21] S. Deville. Freeze-casting of porous ceramics: a review of current achievements and issues, Advanced Engineering Materials 10 (3) (2008) 155-169. https://doi.org/10.1002/adem.200700270
[22] C. Hong, J. Du, J. Liang, X. Zhang, J. Han. Functionally graded porous ceramics with dense surface layer produced by freeze-casting. Ceramics International 37 (2011) 3717-3722.
[23] H. Sun, Y. Chen, F. Chen, Y. Zhang, M. Liu, High-performance solid oxide fuel cells based on a thin La0.8Sr0.2Ga0.8Mg0.2O3−δ electrolyte membrane supported by a nickel-based anode of unique architecture, Journal of Power Sources. 301 (2016) 199–203. https://doi.org/10.1016/j.jpowsour.2015.10.008.
[24] D. Panthi, N. Hedayat, T. Woodson, B.J. Emley, Y. Du, Tubular solid oxide fuel cells fabricated by a novel freeze casting method, Journal of the American Ceramic Society. 103 (2020) 878–888. https://doi.org/10.1111/jace.16781.
[25] F. Schulze-Küppers, U.V. Unije, H. Blank, M. Balaguer, S. Baumann, R. Mücke, W.A. Meulenberg, Comparison of freeze-dried and tape-cast support microstructure on high-flux oxygen transport membrane performance, Journal of Membrane Science. 564 (2018) 218–226. https://doi.org/10.1016/j.memsci.2018.07.028.
[26] Y. Zou, C. Gaudillere, J.E. Escribano, J.M. Serra, J. Malzbender, Microstructure, mechanical behavior and flow resistance of freeze-cast porous 3YSZ substrates for membrane applications,

Journal of the European Ceramic Society. 37 (2017) 3167–3176. https://doi.org/10.1016/j.jeurceramsoc.2017.03.056.
[27] L. Baharudin, M. Watson, Monolithic substrate support catalyst design considerations for steam methane reforming operation, Reviews in Chemical Engineering. 34 (4)(2017) 481-501. https://doi.org/10.1515/revce-2016-0048.
[28] J. Kim, V. Nese, J. Joos, K. Jeske, N. Duyckaerts, N. Pfänder, G. Prieto, Directional freeze-cast hybrid-backbone meso-macroporous bodies as micromonolith catalysts for gas-to-liquid processes, J. Mater. Chem. A. 6 (2018) 21978–21989. https://doi.org/10.1039/C8TA07512C.
[29] A. Trovarelli, Catalytic Properties of Ceria and CeO2-Containing Materials, Catalysis Reviews. 38 (1996) 439–520. https://doi.org/10.1080/01614949608006464.
[30] A. Trovarelli, C. de Leitenburg, M. Boaro, G. Dolcetti, The utilization of ceria in industrial catalysis, Catalysis Today. 50 (1999) 353–367. https://doi.org/10.1016/S0920-5861(98)00515-X.
[31] N. Laosiripojana, W. Sutthisripok, P. Kim-Lohsoontorn, S. Assabumrungrat, Reactivity of Ce-ZrO2 (doped with La-, Gd-, Nb-, and Sm-) toward partial oxidation of liquefied petroleum gas: Its application for sequential partial oxidation/steam reforming, International Journal of Hydrogen Energy. 35 (2010) 6747–6756. https://doi.org/10.1016/j.ijhydene.2010.04.095.
[32] M. Godinho, R. de F. Gonçalves, E.R. Leite, C.W. Raubach, N.L.V. Carreño, L.F.D. Probst, E. Longo, H.V. Fajardo, Gadolinium-doped cerium oxide nanorods: novel active catalysts for ethanol reforming, J Mater Sci. 45 (2010) 593–598. https://doi.org/10.1007/s10853-009-3932-7.
[33] D. Simwonis, H. Thülen, F.J. Dias, A. Naoumidis, D. Stöver, Properties of Ni/YSZ porous cermets for SOFC anode substrates prepared by tape casting and coat-mix® process, Journal of Materials Processing Technology. 92–93 (1999) 107–111. https://doi.org/10.1016/S0924-0136(99)00214-9.
[34] A. Gondolini, E. Mercadelli, P. Pinasco, C. Zanelli, C. Melandri, A. Sanson, Alternative production route for supporting La0.8Sr0.2MnO3−δ-Ce0.8Gd0.2O2−δ (LSM-GDC), International Journal of Hydrogen Energy, 37 (2012) 8572–8581. https://doi.org/10.1016/j.ijhydene.2012.02.091.
[35] F. Basile, R. Mafessanti, A. Fasolini, G. Fornasari, E. Lombardi, A. Vaccari, Effect of synthetic method on CeZr support and catalytic activity of related Rh catalyst in the oxidative reforming reaction, Journal of the European Ceramic Society, 39 (2019) 41–52. https://doi.org/10.1016/j.jeurceramsoc.2018.01.047.
[36] A. Fasolini, S. Abate, D. Barbera, G. Centi, F. Basile, Pure H2 production by methane oxy-reforming over Rh-Mg-Al hydrotalcite-derived catalysts coupled with a Pd membrane, Applied Catalysis A: General. 581 (2019) 91–102. https://doi.org/10.1016/j.apcata.2019.05.024.
[37] F. Basile, P. Benito, G. Fornasari, M. Monti, E. Scavetta, D. Tonelli, A. Vaccari, Novel Rh-based structured catalysts for the catalytic partial oxidation of methane, Catalysis Today, 157 (2010) 183–190. https://doi.org/10.1016/j.cattod.2010.04.039.
[38] A. Ballarini, F. Basile, P. Benito, I. Bersani, G. Fornasari, S. Miguel, S.C.P. Maina, I.M.J. Vilella, A. Vaccari, O. Scelza, Platinum supported on alkaline and alkaline earth metal-doped alumina as catalysts for dry reforming and partial oxidation of methane, Applied Catalysis A: General, 433–434 (2012) 1–11. https://doi.org/10.1016/j.apcata.2012.04.037.
[39] R. Moreno, Better ceramics through colloid chemistry, Journal of the European Ceramic Society. 40 (2020) 559–587. https://doi.org/10.1016/j.jeurceramsoc.2019.10.014.
[40] A. Gondolini, E. Mercadelli, V. Zin, S. Barison, A. Sanson, Easy preparation method of stable copper-based nanoparticle suspensions in lubricant engine oil, Lubrication Science. 32 (5) (2020) 205-217. https://doi.org/10.1002/ls.1496.
[41] M. Kaszuba, D. McKnight, M.T. Connah, F.K. McNeil-Watson, U. Nobbmann, Measuring sub nanometre sizes using dynamic light scattering, J Nanopart Res. 10 (2008) 823–829. https://doi.org/10.1007/s11051-007-9317-4.

[42] J.M. Rodríguez-Parra, R. Moreno, I.M. Nieto, Effect of cooling rate on the microstructure and porosity of alumina produced by freeze casting, Journal of the Serbian Chemical Society. 77 (2012) 1775–1785.
[43] Y. Liu, W. Zhu, K. Guan, C. Peng, J. Wu, Freeze-casting of alumina ultra-filtration membranes with good performance for anionic dye separation, Ceramics International. 44 (2018) 11901–11904. https://doi.org/10.1016/j.ceramint.2018.03.160.
[44] A.M.A. Silva, E.H.M. Nunes, D.F. Souza, D.L. Martens, J.C. Diniz da Costa, M. Houmard, W.L. Vasconcelos, Effect of titania addition on the properties of freeze-cast alumina samples, Ceramics International. 41 (2015) 10467–10475. https://doi.org/10.1016/j.ceramint.2015.04.132.
[45] J.R. Rostrup-Nielsen, Catalytic Steam Reforming, in: J.R. Anderson, M. Boudart (Eds.), Catalysis: Science and Technology Volume 5, Springer, Berlin, Heidelberg, 1984: pp. 1–117. https://doi.org/10.1007/978-3-642-93247-2_1.
[46] J. Xu, G.F. Froment, Methane steam reforming, methanation and water-gas shift: I. Intrinsic kinetics, AIChE Journal. 35 (1989) 88–96. https://doi.org/10.1002/aic.690350109.
[47] B. Li, K. Maruyama, M. Nurunnabi, K. Kunimori, K. Tomishige, Temperature profiles of alumina-supported noble metal catalysts in autothermal reforming of methane, Applied Catalysis A: General. 275 (2004) 157–172. https://doi.org/10.1016/j.apcata.2004.07.047.
[48] B. Li, S. Kado, Y. Mukainakano, M. Nurunnabi, T. Miyao, S. Naito, K. Kunimori, K. Tomishige, Temperature profile of catalyst bed during oxidative steam reforming of methane over Pt-Ni bimetallic catalysts, Applied Catalysis A: General. 304 (2006) 62–71. https://doi.org/10.1016/j.apcata.2006.02.025.
[49] T. Giroux, S. Hwang, Y. Liu, W. Ruettinger, L. Shore, Monolithic structures as alternatives to particulate catalysts for the reforming of hydrocarbons for hydrogen generation, Applied Catalysis B: Environmental. 56 (2005) 95–110. https://doi.org/10.1016/j.apcatb.2004.07.013.
[50] T. V. Choudhary, V.R. Choudhary. “Energy-efficient syngas production through catalytic oxy-methane reforming reactions.” Angewandte Chemie International Edition 47 (10) (2008) 1828-1847

Figure Caption

Figure 1. Mean particle size of the powder-deflocculant suspension evaluated using DLS analysis.

Figure 2. SEM micrographs of the GDC 20 powder used in this study.

Figure 3. Viscosity values of the GDC 20 slurries containing the different deflocculants.

Figure 4. Viscosity of the GDC 20 slurries a) and mean size of the suspensions b) containing different amounts of Phospholan PE65.

Figure 5. SEM micrographs of the a) polished and b) fresh fracture of the sample produced by directional freeze casting.

Figure 6. SEM micrographs of the polished (on the left) and fresh fracture (on the right) at different height of the freeze cast sintered sample.

Figure 7. SEM micrographs of the polished fractures of the bottom part of samples frozen at a) 0°C, b) 5°C and c) 35°C. Figure d) is a fresh fracture of the sample frozen at 35°C.

Figure 8. SEM micrographs of the polished fractures of the upper part of samples frozen at 35°C a) in air, b) in camphene saturated chamber and c) in water bath.

Figure 9. Pore size distribution a) and Darcy permeability values b) of the produced samples

Figure 10. Methane conversion, equilibrium methane conversion and hydrogen production obtained at S/C 0.70, O/C 0.21, 1 atm, and different temperatures.

Figure 11. Methane conversion, equilibrium methane conversion and hydrogen production obtained at 750°C, O/C 0.21, 1 atm, and S/C.

Figure 12. Catalytic bed temperature profile at different conditions varying the oven temperature (a) and the catalyst (b).

Table Caption

Table 1. Operative conditions employed in the catalytic tests.

Table 2. Values of porosity, mean pore diameter and permeability of the produced samples.

Table 3. Experimental and equilibrium conversion obtained by the catalytic membrane and pelleted catalyst in oxy-reforming at 750°C with S/C 0,7 and O/C 0,2 or S/C 0,5 and O/C 0,5.